Available online at www.sciencedirect.com
ScienceDirect
Catalysis Today 117 (2006) 394–406
CATALYSIS TODAY
www.elsevier.com/locate/cattod

Understanding and modeling of thermofluidic processes in catalytic combustion

John Mantzaras *

Paul Scherrer Institute, Combustion Research, CH-5232 Villigen PSI, Switzerland

Available online 2 August 2006

Abstract

Recent advances in the modeling of chemistry and transport in catalytic combustion, which have been fostered by complementary developments in in situ measurements of gas-phase thermoscalars, are reviewed. Key issues such as the implementation of proper sub-models for surface kinetics, low temperature gas-phase kinetics and interphase transport are presented, with emphasis on fuel-lean and fuel-rich steady catalytic combustion. The advent of in situ measurements of major and minor gas-phase species concentrations over the catalyst boundary layer has led to reactor configurations that can tolerate large transverse gradients thus allowing for kinetic investigations at high temperatures and realistic reactant compositions. It is shown that those measurements, when used in conjunction with multidimensional modeling, can elucidate the underlying hetero-/homogeneous kinetics and their interactions at industrially-relevant operating conditions. Turbulent transport, an issue of particular interest in gas-turbines, is also addressed. Experiments and simulations have shown that key to the aptness of near-wall turbulence models is their capacity to capture the strong flow laminarization induced by the heat transfer from the hot catalytic walls. New modeling directions that include direct numerical simulation (DNS) for transient catalytic combustion and lattice Boltzmann (LB) discrete velocity models for intraphase transport are briefly outlined.

Keywords: Heterogeneous and homogeneous kinetics; Numerical modeling; Turbulent catalytic combustion

1. Introduction

Catalytic processes have received increased attention in numerous industrial applications that include chemical synthesis, exhaust gas aftertreatment, and heat/power generation systems. The progress in the last systems depends on crucial advances in catalyst technology and in multidimensional numerical modeling needed for reactor design. The numerical models require salient description of the catalytic and gas-phase kinetics and of the interphase fluid mechanical transport. Moreover, the employed reaction schemes should be valid over a wide range of operating conditions, e.g. from atmospheric pressure in household burners and industrial boilers, to ~5 bar in microreactors and, finally, to ~15 bar in large stationary turbines. Recent advances in the thermofluidic modeling of hetero-/homogeneous processes are reviewed, in light of accompanying developments in experimental techniques that have yielded direct in situ gas-phase thermoscalar measurements over the catalyst boundary layer.

The advent of in situ spatially-resolved measurements of major and minor gas-phase species concentrations over the catalyst [1–4] using spontaneous Raman and laser induced fluorescence (LIF), respectively, has fostered fundamental kinetic studies at high temperatures (>1000 °C) and realistic reactant compositions. It is demonstrated that the combination of in situ measurements with multidimensional modeling can lead to the development and/or refinement of catalytic and gas-phase reaction schemes at industrially-relevant operating conditions. The methodology is first demonstrated with fuel-lean combustion of CH_4/air and H_2/air mixtures over Pt at 1 bar $\leq p \leq$ 16 bar [3–7]. The impact of radical adsorption/desorption reactions and of heterogeneously-formed major products on gaseous combustion is elucidated. Fuel-rich catalytic combustion of methane over Rh [8,9] follows suit, using the same experimental/numerical methodology.

Turbulent transport, an issue of prime interest in gas-turbines that use catalytically stabilized combustion (CST), is discussed with the aid of modeling and in situ experiments [10–12]. It is

* Tel.: +41 56 3104046; fax: +41 56 3102199.
E-mail address: ioannis.mantzaras@psi.ch.

0920-5861/$ – see front matter © 2006 Elsevier B.V. All rights reserved.
doi:10.1016/j.cattod.2006.06.047

Nomenclature

c_μ	turbulence constant
f_μ	damping function
k	turbulent kinetic energy
S_φ	source term for variable φ
u, v	streamwise and transverse velocity components
Greek symbols	
ε	dissipation rate of turbulent kinetic energy
μ_t	turbulent viscosity
ρ	density
σ_φ	turbulent Prandtl or Schmidt number
φ	scalar variable or fuel-to-air equivalence ratio
Γ_l, Γ_{eff}	laminar and effective turbulent transport coefficients
Superscripts	
$\sim$	Favre average
$-$	Reynolds average
Subscripts	
ag	appreciable gaseous conversion
ig	appreciable gaseous conversion, homogeneous ignition

shown that crucial for the correct prediction of the in-channel turbulence levels is the capture of the strong flow laminarization induced by the hot catalytic surfaces. Finally, new modeling directions that include direct numerical simulation (DNS) and lattice Boltzmann (LB) approaches are presented. The former is particularly promising for catalytic ignition and kinetically–driven dynamic oscillatory phenomena, and the latter for improving intraphase diffusion models.

2. In situ experiments

The development of suitable catalytic and low-temperature gas-phase chemical reaction schemes is prerequisite to the full exploitation of advanced multidimensional numerical models. Even though in situ surface science diagnostics have progressed considerably during the last years [13,14], they have not yet advanced to a standard research tool for industrially-relevant pressures and temperatures, for technical catalysts and, finally, for surfaces exposed to the full array of hydrocarbon combustion products. Thus, the development of surface reaction mechanisms relies heavily on additional experiments carried out in a variety of laboratory-scale reactors. Those supplementary measurements aim at introducing appropriate kinetic rate modifications so as to bridge the pressure and materials gap of the mainly ultra high vacuum (UHV) surface science experiments.

A number of reactor designs have been hitherto established for assessing surface kinetics. The most widely used configuration is the nearly isothermal, low-temperature ($T \lesssim 600\ ^\circ$C), gradientless (in the radial direction) microflow reactor, which is fed with highly-diluted fuel/oxidizer mixtures in order to maintain a minimal temperature rise. Even though the modeling of such reactors is simple, the low temperature rise poses inherent limitations for the description of thermally controlled processes. In addition, high temperature investigations are hindered since very large gas hourly spatial velocities (GHSV) are needed to remove mass transport limitations. Recent improvements include the microflow annular [15,16] and the linear reactors [17], where the flow is forced through sub-millimeter narrow channels such that the resulting high linear velocities alleviate mass transport limitations. Another popular configuration is the stagnation flow (SF) reactor, which has provided a wealth of data on catalytic ignition/extinction, steady fuel conversion and product selectivity under realistic temperatures and mixture compositions [18–22]. SF reactors can operate with large gas-phase gradients, the reason being that modeling with well-established 1D codes [23] is nowadays straightforward even for complex reaction schemes. The variables measured in both microflow and SF reactors are typically global and not local. Due to size limitations, only the inlet and exit composition and the overall reactor temperature can be monitored in microflow reactors. Stagnation-flow experiments have also provided mainly global quantities (total fuel conversion, product selectivity, autothermal behavior, ignition/extinction), despite the fact that the geometry itself is particularly amenable to spatially-resolved measurements. Local measurements across stagnation-flow boundary layers have advanced only recently and were obtained with intrusive [22] as well as non-intrusive techniques [24]. The advantage of local measurements is discussed next within the context of optically accessible reactors.

A new type of reactor suitable for kinetic studies is the optically-accessible, high-pressure, high-temperature, steady-flow reactor of Fig. 1 [2,3,5,6,11]. The test rig consists of a rectangular channel-flow reactor and a high-pressure tank. The reactor comprises two horizontal Si[SiC] ceramic plates (300-mm long, 104 mm wide, placed 7 mm apart) and two vertical quartz windows. The inner Si[SiC] surfaces are coated with the catalyst of interest. The surface temperature (T_W) along the x–y symmetry plane is measured by thermocouples embedded 0.9 mm beneath the catalyst. Optical accessibility is maintained from both reactor sides via two high–pressure quartz windows positioned on the tank. An additional counterflow streamwise optical access is also provided. In situ, laser-based spectroscopic measurements are applied (see Fig. 1) and include: 1D spontaneous Raman of major gas-phase species concentrations and temperature across the entire 7-mm channel height and planar LIF of trace species (typically OH in fuel-lean and CH_2O in fuel-rich hydrocarbon combustion) along the x–y symmetry plane. Fluid mechanical transport, in particular turbulent, can also be assessed with particle image velocimetry (PIV) [12]. Thus, both chemistry and transport can be investigated in this laboratory reactor.

The set-up of Fig. 1 has a number of advantages originating either from the reactor geometry itself or from the in situ nature of the measurements. The 2D channel configuration allows for investigating certain aspects of ignition (heterogeneous or homogeneous) at steady operating conditions since the streamwise coordinate can also serve as

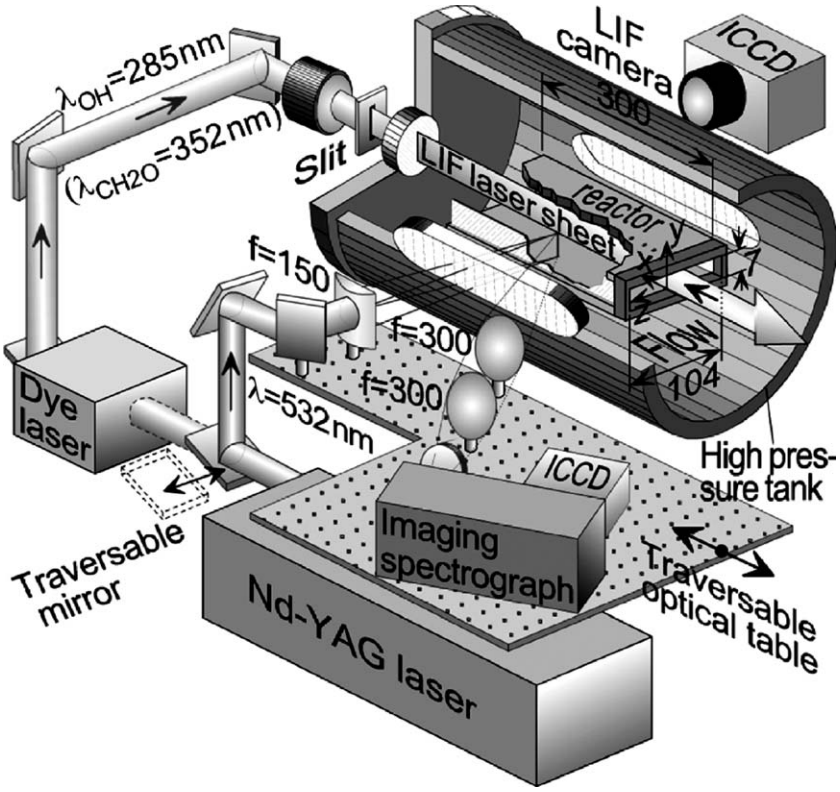

Fig. 1. Optically accessible catalytic reactor and Raman/LIF setup. All lengths are in mm.

time axis. In contrast, ignition in stagnation flows is always an abrupt transient event. Since radial gradients can be tolerated, catalytic reactivity studies can be carried out at high surface temperatures (up to 1350 K) without the need of excessively large GHSV. Moreover, the set-up is well-suited for the investigation of the hetero-/homogeneous chemistry coupling since gaseous combustion is contained inside the catalytic channel rather than in a follow-up burnout zone. Nonetheless, those benefits come at an increasing experimental and numerical complexity. Two-dimensional CFD models, such as those of Refs. [10,25] are required to simulate the in situ experiments.

3. Kinetic scheme validation

3.1. Fuel-lean methane/air combustion over Pt

The establishment of suitable catalytic and gaseous kinetics for fuel-lean ($\varphi < 0.4$) combustion of CH_4/air mixtures over polycrystalline Pt at pressures up to 16 bar is presented next. The catalytic reactivity is assessed first by comparing Raman-measured and predicted species boundary layer profiles. Gas-phase combustion is then investigated using both Raman and OH-LIF. The hetero-/homogeneous pathway coupling follows suit and the operating regimes where one reaction pathway dominates over the other are delineated. Finally, the kinetic model is applied to a prototype turbine catalytic reactor.

3.1.1. Heterogeneous kinetics

The methodology for assessing the catalytic reactivity from the Raman data is presented in Fig. 2. The first step involves the delineation of the reactor extent over which the contribution of the gaseous pathway is negligible. Fig. 2a provides the catalytic (C) and gas-phase (G) methane conversions computed with the elementary catalytic and gas-phase schemes of Deutschmann [26] and Warnatz [27], respectively (the suitability of the latter is discussed in Section 3.1.2). The volumetric G conversion has been integrated across the 7-mm transverse distance so as to facilitate comparisons with the surface C conversion. The position of appreciable gas-phase conversion (x_{ag}), where G amounts to 5% of the C, is not associated with the onset of homogeneous ignition: it will be shown next that appreciable gas-phase methane conversion can still occur without significant homogeneous exothermicity. The Raman-measured transverse species profiles are then compared against the simulations (Fig. 2b) only at $x < x_{ag}$ in order to avoid falsification of the surface kinetics by the gas-phase chemistry. Key to those comparisons is the attainment of kinetically controlled conversion, which is manifested in Fig. 2b by the non-zero CH_4 levels at both walls. The good agreement in the comparisons of Fig. 2b reflects the aptness of the employed catalytic scheme. Detailed studies have further shown [2] that the catalytic reactivity increases with increasing pressure and that the employed scheme [26] is suitable for 1 bar $\leq p \leq$ 16 bar and 780 K $\leq T_W \leq$ 1250 K. Investigations with other reaction schemes [2] reveal that key to the suitability of any surface mechanism is its capacity to capture the reduction in

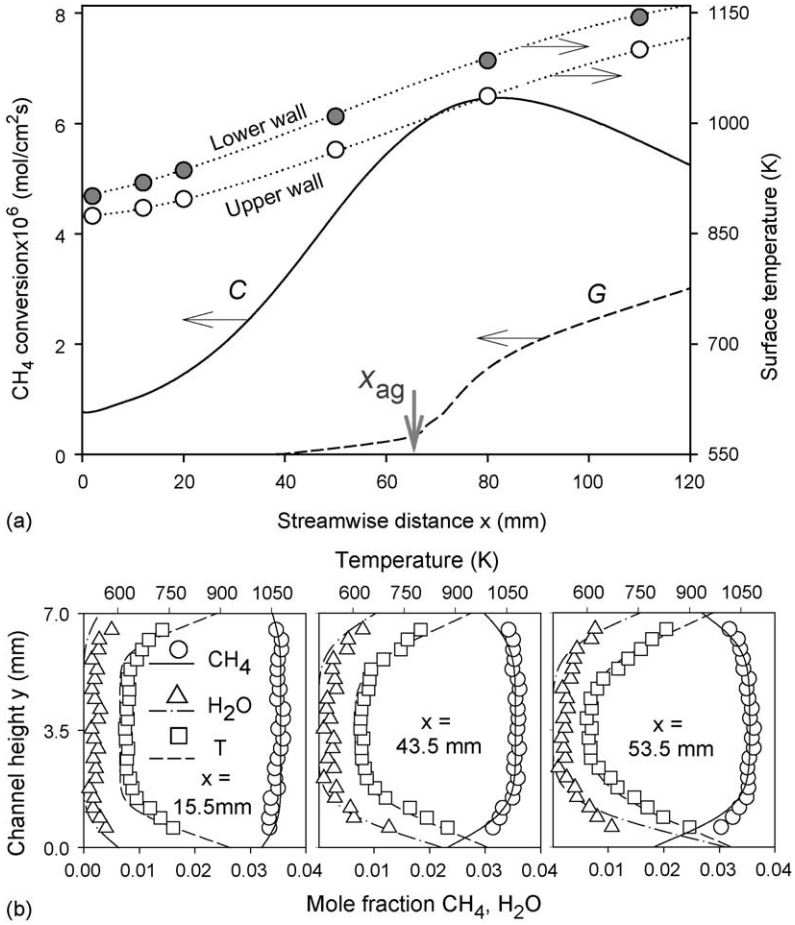

Fig. 2. Methane/air combustion over Pt. (a) Computed axial profiles of catalytic (C) and gaseous (G) CH_4 conversion for $p = 14$ bar, $\varphi = 0.35$, $T_{IN} = 606$ K and $U_{IN} = 0.55$ m/s (adapted from [2]). The vertical arrow defines the location of appreciable gaseous contribution (x_{ag}). Measured surface temperatures are also provided. (b) Predicted (lines) and measured (symbols) transverse profiles of species mole fractions and temperature.

surface free sites with rising pressure that, in turn, restrains the rate of increase of the catalytic reactivity with increasing pressure [2]. The methane catalytic reaction rate scales as p^{1-n}, where $0 < 1-n < 1$ and the exponent n is itself a function of pressure. The aptness of the employed scheme [26] at high pressures stems from the inclusion of a CH_4 adsorption rate that has an order of 2.3 with respect to Pt. The above pressure dependence has particular implications for reactor design as will be discussed in Section 3.1.3.

The carbon flux of Fig. 3 (pertaining to the conditions of Fig. 2) indicates that methane is converted in parallel by both reaction pathways. Methane is oxidized in the gas-phase to CO, which is adsorbed very efficiently on Pt due to its high sticking coefficient. The adsorbed CO(s) is oxidized catalytically to CO_2(s) that further desorbs to the gas-phase. Gas-phase hydrocarbon combustion can generally be described by a two-step process, the first being an incomplete reaction to CO and the second the main exothermic oxidation of CO to CO_2 [28]. The catalytic pathway clearly inhibits the onset of homogeneous ignition by depriving CO from the gas-phase. Nonetheless, even in the absence of homogeneous ignition, the gaseous pathway can amount to significant methane conversion (particularly at higher pressures) through the incomplete

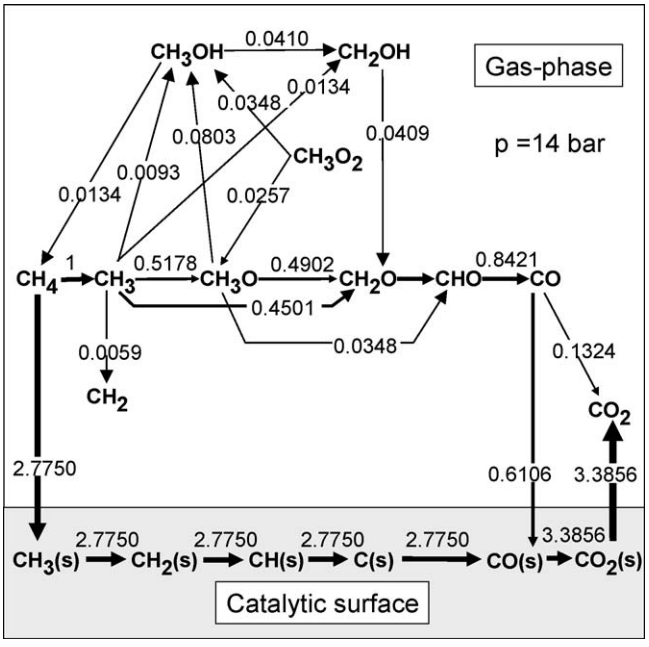

Fig. 3. Catalytic and gas-phase carbon reaction flux for the case of Fig. 2 at $x = 95$ mm (adapted from [2]). Only fluxes greater than 0.004 are shown.

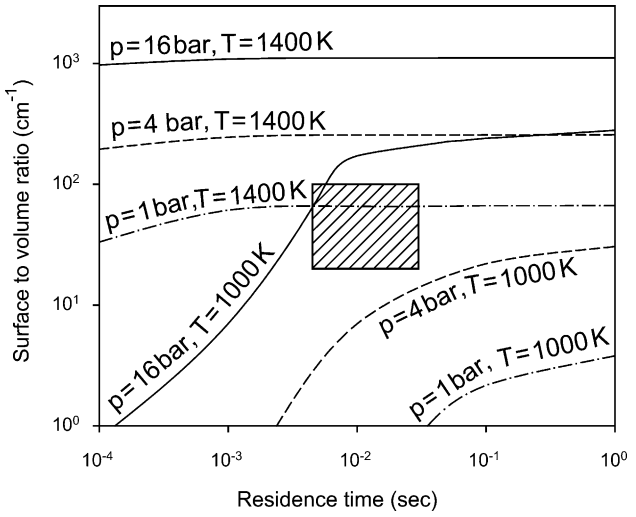

Fig. 4. Regimes of significance of the gaseous reaction pathway in CH_4/air combustion over Pt (adapted from [2]). The areas above each line of constant pressure and temperature delineate the zones where the gas-phase chemistry can be neglected. The shaded area is an estimate of CST-based turbine reactor operating regimes.

oxidation of CH_4 to CO. The regimes of importance for the gaseous pathway are delineated in the parametric plot of Fig. 4, which was constructed using a surface perfectly stirred reactor (SPSR) model [29] and the hetero-/homogeneous schemes of Deutschmann/Warnatz. In the zones below each line of fixed pressure and temperature, the gas-phase chemistry cannot be neglected as it amounts to more than 5% of the total conversion. Fig. 4 provides only a rough assessment of the regimes of significant gas-phase contribution since interphase or intraphase diffusion limitations have not been accounted for. The shaded rectangle is an estimate of the regimes of CST-based turbines. It is seen that the gaseous pathway cannot be neglected at turbine-relevant conditions ($p \geq 16$ bar and $T \geq 1000$ K). This is also attested by additional 2D CFD computations in realistic systems. For example, in a channel with a diameter of 1 mm, a length of 100 mm, $T_{IN} = 673$ K, $U_{IN} = 5$ m/s, $p = 16$ bar and a wall temperature $T_W = 1200$ K, the predictions yield (in the absence of homogeneous ignition) an 84% total methane conversion, out of which 74% is catalytic and 10% gaseous.

3.1.2. Homogeneous kinetics

Homogeneous kinetics have been studied at 1 bar $\leq p \leq$ 16 bar and 1050 K $\leq T_W \leq$ 1430 K [4-7]. It has been recently established [3,7] that the combination of OH LIF and Raman is well-suited for the validation of gas-phase schemes as it allows for simultaneous investigation of both reaction pathways. An assessment of the catalytic processes preceding the onset of homogeneous ignition is still necessary: even though the catalytic scheme [26] has been validated in Section 3.1.1, the relatively high surface temperatures required to achieve homogeneous ignition can possibly deactivate (totally or partially) the catalyst. This leads to a near-wall fuel excess that can, in turn, promote the onset of homogeneous ignition and thus falsify the gaseous kinetics. An additional complication arises from the existence of infinite combinations of catalytic and gaseous reactivities yielding exactly the same homogeneous ignition distance [30]. Therefore, the Raman measurements remove any uncertainties associated with the catalytic pathway that can potentially interfere with the evaluation of gaseous chemistry.

Measured and predicted 2D OH distributions are shown in Fig. 5A. Raman-measured and predicted species profiles for Case 3 of Fig. 5A are given in Fig. 5B and indicate a catalytic operation close to the mass-transport-limit. The gas-phase scheme of Warnatz [27] captures the measured homogeneous ignition position (x_{ig}) and the ensuing flame sweep angles for $p \geq 6$ bar (Fig. 5A). Moreover, in conjunction with the scheme of Deutschmann, it reproduces the gas-phase contribution in the combined hetero-/homogeneous conversion zone $x_{ag} \leq x \leq x_{ig}$ (e.g. Fig. 5B(b)). On the other hand, GRI-3.0 [31] and Leeds [32] underpredict substantially the measured x_{ig} at all pressures. Ignition delay times were computed as $\tau_d = \tau(x_{ig})(\tau(x) = \int_0^x \mathrm{d}x/\bar{U}(x)$ with $\bar{U}(x)$ the mean axial velocity) using the three gas-phase schemes and the resulting differences in τ_d were up to 100 ms. Since residence times in turbine reactors are typically less than 30 ms, it is evident that the burner design can be greatly impacted by the choice of reaction mechanism. Detailed analysis of the three mechanisms has shown [7] that the differences in Fig. 5A are attributed to both the low equivalence ratios and the low temperatures. The first factor bears the direct impact of the catalytic pathway, which depletes methane such that the effective equivalence ratio at x_{ig} is considerably lower than the (already low) inlet value. The second factor reflects the particular operational conditions of catalytic systems and it impacts the relative contribution of the different oxidation routes of methane. The capacity of the various schemes to reproduce x_{ig} is directly related to their suitability in predicting ignition delay times. On the other hand, the post-ignition behavior of the gaseous schemes reflects their ability to capture propagation characteristics (i.e. the flame sweep angles in Fig. 5A). The former is far more important than the latter since the onset of gaseous combustion is detrimental to the catalyst and/or reactor integrity and numerical models should be able to predict the likelihood of such an event.

Being suitable at 6 bar $\leq p \leq$ 16 bar, the scheme of Warnatz [27] provides a platform for an amended mechanism valid over the extended range 1 bar $\leq p \leq$ 16 bar. Sensitivity analysis reveals that at $p = 1$ bar the homogeneous ignition is particularly sensitive to the chain branching step CHO + M = CO + H + M, while at $p = 16$ bar the corresponding sensitivity is weak. Friedrichs et al. [33] has recently suggested slower kinetic rates for this step. To improve the predictions of Fig. 5A at $p < 6$ bar, the pre-exponential of this reaction was reduced by a factor of 1.8 in scheme of Warnatz. The altered elementary scheme provided good agreement with the OH LIF data over 1 bar $\leq p \leq$ 16 bar [4].

The coupling of hetero-/homogeneous chemistry is addressed next using the validated schemes of Deutschmann and the amended Warnatz. OH radicals are produced upstream by the catalyst (i.e. the resulting OH fluxes are net desorptive). It would, therefore, appear that the catalytically-formed OH promotes gaseous combustion by accelerating the main fuel

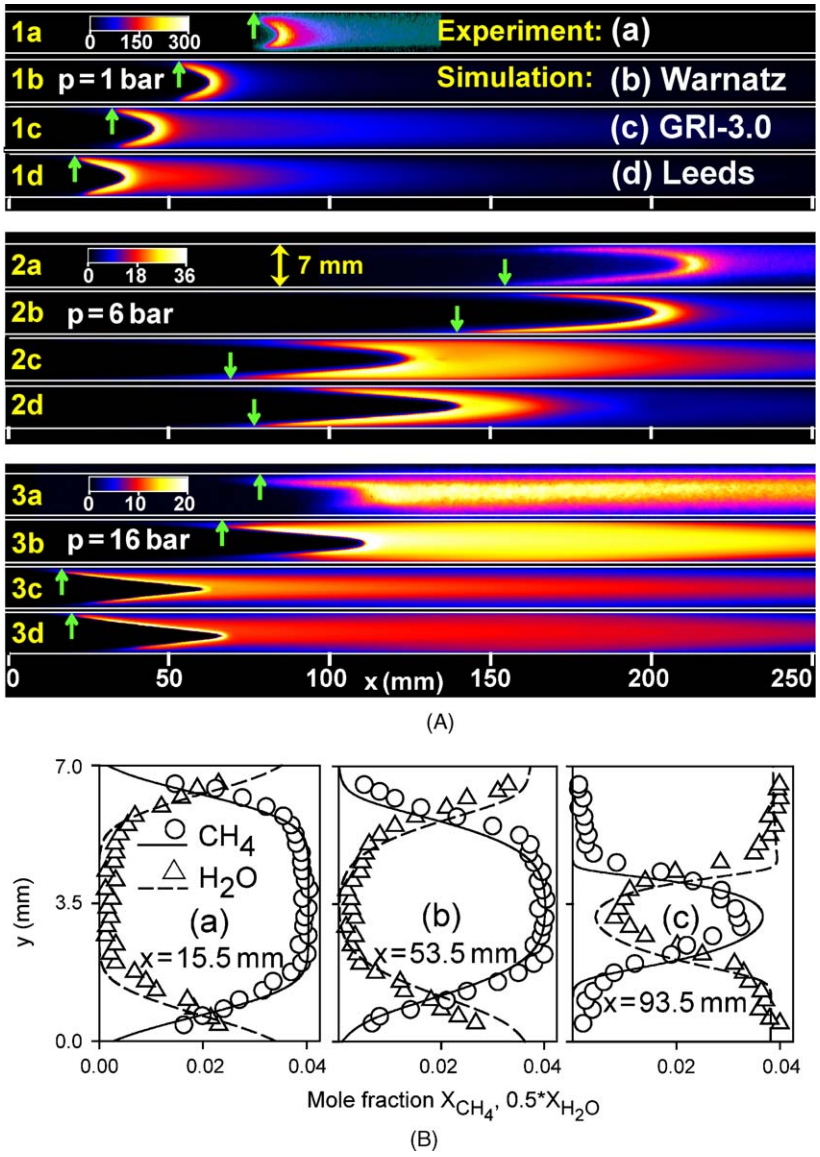

Fig. 5. (A): LIF-measured (a) and numerically predicted (b, c and d) OH maps in CH_4/air combustion over Pt (adapted from [5,7]). The color bars provide the OH in ppmv. (1) p = 1 bar, φ = 0.31, T_{IN} = 754 K; (2) p = 6 bar, φ = 0.36, T_{IN} = 569 K and (3) p = 16 bar, φ = 0.40, T_{IN} = 643 K. The catalytic scheme of Deutschmann [26] and the gas-phase schemes of: (b) Warnatz [27], (c) GRI-3.0 [31], and (d) Leeds [32] were used. The arrows denote the onset of homogeneous ignition. (B) Raman-measured (symbols) and predicted (lines, using the Deutschmann/Warnatz schemes) transverse profiles of species mole fractions for Case 3 of (A).

attack step $CH_4 + OH = CH_3 + H_2O$ (see also Fig. 3). Nonetheless, the heterogeneous OH fluxes are too low to have a noticeable impact on gaseous chemistry. This is shown by removing the OH adsorption/desorption reactions and computing anew: the gaseous chemistry is still able to build the radical pool without the aid of the heterogeneous pathway. Therefore, the catalyst itself is a poor source of OH radicals so as to meaningfully affect the gaseous pathway at conditions away from homogeneous ignition. On the other hand, at the late stages of the gaseous induction zone or at post-ignition positions, the catalyst turns to a sink of OH (the OH fluxes become net adsorptive). This behavior determines an overall mild inhibition of homogeneous ignition: x_{ig} decreases by ~10% when both OH adsorption/desorption reactions are removed. The stabilization of gaseous combustion in CST systems should be thus attributed mainly to thermal and not to radical interactions of the two pathways. Finally, experiments and simulations [4] have shown that the catalytically-formed H_2O promotes chemically the onset of homogeneous ignition.

3.1.3. Application to a gas-turbine catalytic reactor

The pressure dependence of the heterogeneous reactivity (see Section 3.1.1) has implications in reactor design. The catalytic combustion of fuel-lean CH_4/air mixtures has been investigated experimentally and numerically [34] in a prototype gas-turbine honeycomb reactor. The structure has a length of 136 mm, channel hydraulic diameter of 1.2 mm and is coated with a Pt-based catalyst. To avoid reactor overheat, catalyst is applied only to alternate channels of the honeycomb (passive cooling). Thermocouples monitor the reactor exit temperature

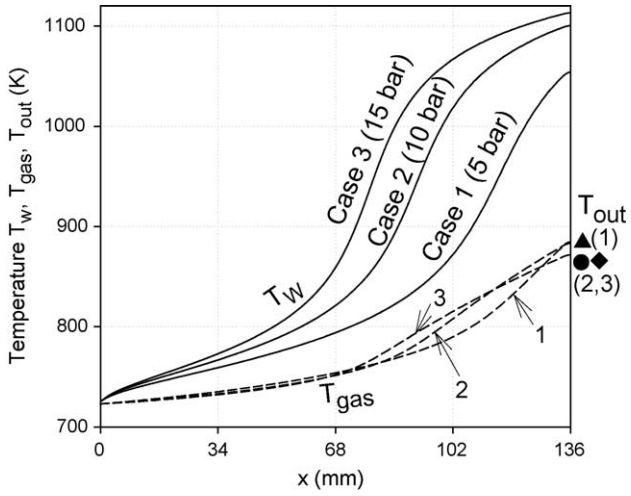

Fig. 6. Axial profiles of computed wall temperatures (T_W, solid lines) and mean gas temperatures (T_{gas}, dashed lines), and measured exit temperatures (T_{out}, symbols) in a Pt-based honeycomb catalytic reactor. (1) $p = 5$ bar, (2) $p = 10$ bar and (3) $p = 15$ bar. In all cases $\varphi = 0.4$, $U_{IN} = 15$ m/s and $T_{IN} = 723$ K. The measured temperature rise ΔT across the reactor is 165, 140 and 142 K for Cases 1–3, respectively. The corresponding computed rise is 162, 160 and 149 K. The simulated mass-transport-limited maximum temperature rise ΔT_{max} is 420, 341 and 288 K for Cases 1–3, respectively.

and the experiments are simulated with a 2D model that includes a simplified surface reaction for this commercial catalyst and the gaseous scheme of Warnatz [27]. Gas-phase chemistry is shown to be negligible since the passive cooling moderates the surface temperatures. Computed surface and mean-gas temperatures as well as measured exit temperatures are shown in Fig. 6 for three pressures and a fixed inlet velocity. Both predictions and measurements indicate that an increase in pressure (and hence in mass throughput) by a factor of three does not alter appreciably the temperature rise ΔT across the reactor or, equivalently, the fractional methane conversion. The theoretically maximum attainable temperature rise ΔT_{max} (corresponding to mass-transport-limited conversion) decreases with increasing mass throughput (see caption of Fig. 6) such that the relative fuel conversion $\Delta T/\Delta T_{max}$ increases with rising pressure. This appears to be contradictory because the fuel conversion in laminar channel flows is, at least under mass-transport-limited operation, inversely proportional to the inlet Reynolds number [30]. The rise in relative fuel conversion with increasing pressure can be readily explained by a very specific interplay of transport, kinetics, and reactor geometry. The dependence of the catalytic reactivity ($\sim p^{1-n}$, $1 > n$) indicates that surface reactions in noble metals accelerate with increasing pressure. Heat and mass transport rates also increase with increasing Reynolds numbers (i.e. pressure) in developing flows. However, for the specific channel geometry the convective heat transfer to the fluid increases at a rate slower than that of the local catalytic heat generation, causing the conversion to increase and the light-off distance to diminish with rising pressure. The latter is evident in Fig. 6 by the increase of the surface temperatures at higher pressures. The attainment of pressure-independent fractional fuel conversion (or ΔT) is highly desirable in turbines since it provides a constant temperature rise across the reactor during pressure ramps and load changes.

3.2. Partial oxidation of methane over Rh

3.2.1. Catalytic and gas-phase kinetics

The catalytic partial oxidation (CPO) of methane is under intense investigation for power generation [35,36]. The methodology set forth in Section 3.1 is applied herein. In contrast to the previous fuel-lean total oxidation studies (where Raman data of only the deficient CH_4 was sufficient to deduce the catalytic reactivity) measurements of all major species are required in CPO due to the presence of multiple and sometimes competing heterogeneous reaction pathways, such as complete and partial oxidation, steam reforming, water gas shift, and CO_2 reforming. Key issues addressed by the Raman measurements are the methane conversion and synthesis gas (CO and H_2) yields. Measured and predicted transverse species profiles during CPO of CH_4/air over Rh/ZrO_2 catalysts at 6 bar have illustrated [8] that, over the reactor extent where oxygen is still available, the elementary catalytic scheme of Deutschmann (Schwiedernoch et al. [37]) provides good agreement to the measured major species mole fractions. In the oxygen-depleted zones of the reactor, however, the heterogeneous scheme overpredicts the impact of steam reforming and water gas shift reactions, resulting in higher computed hydrogen yields. The spatially-resolved nature of the Raman measurements allows for the evaluation of the local rates of species production/destruction and hence for the determination of the streamwise evolution of the controlling reactions [8]. Recent comparisons between LIF-measured and predicted 2D distributions of CH_2O [38] suggest that the C2 gas-phase scheme of Warnatz [27] and the catalytic scheme of Deutschmann [37] reproduce the onset of homogeneous ignition.

3.2.2. Application of CPO to power generation systems

The CPO of CH_4/O_2 mixtures diluted with exhaust gas recycle has been investigated [9] in a short contact time (~8 ms) prototype turbine honeycomb reactor similar to that used in the fuel-lean application of Fig. 6. The reactor is always operated with an oxygen breakthrough and the feed comprises 20.4 vol.% CH_4, 10.2 vol.% O_2, 46.3 vol.% H_2O and 23.1 vol.% CO_2. The operating conditions are $p = 5$ bar, $T_{IN} = 623$ K and $U_{IN} = 5$ m/s. The reactor length is 75 mm (only the central 55 mm are coated) and the channel hydraulic diameter is 1.2 mm. Thermocouples and gas chromatography provide the reactor temperature and exhaust gas composition. Two-dimensional CFD predictions with the hetero-/homogeneous schemes discussed in Section 3.2.1 indicate that gas-phase chemistry is negligible. Axial profiles of the predicted wall temperature (T_W), the mean gas temperature (T_{gas}) and methane and hydrogen mole fractions are depicted in Fig. 7. In the same figure, the measured temperatures along the reactor and the measured mole fractions of CH_4 and H_2 at the exit are provided along with the calculated adiabatic equilibrium temperature and CH_4 and H_2 mole fractions.

A good agreement is attained between measured and predicted exit compositions and reactor temperatures (the

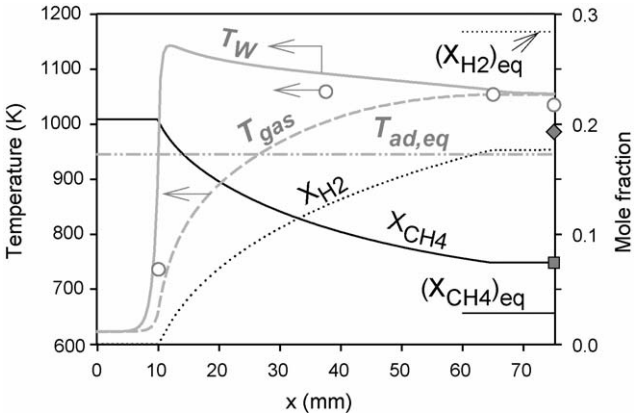

Fig. 7. Axial profiles of temperature and species mole fractions in partial oxidation of methane. Computations: wall temperature T_W (solid gray lines), mean gas temperature T_{gas} (dashed gray lines), mean CH_4 mole fraction (black solid lines), mean H_2 mole fraction (black dotted lines). Adiabatic equilibrium calculations: gas temperature ($T_{ad,eq}$, dashed-double-dotted gray lines) and CH_4 and H_2 mole fractions. Measurements: temperature (open circles), outlet H_2 mole fraction (filled diamond), outlet CH_4 mass fraction (filled square). The coated section of the reactor extends over 10 mm $\leq x \leq$ 65 mm.

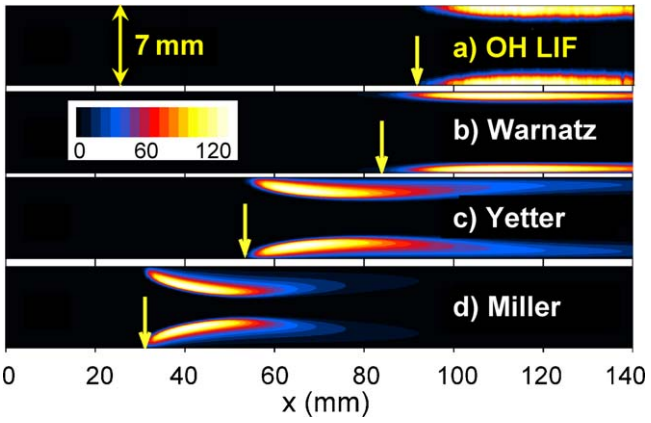

Fig. 8. Hydrogen/air combustion over Pt. LIF-measured (a) and numerically predicted (b, c and d) distributions of the OH radical in the reactor of Fig. 1: $p = 1$ bar, $\varphi = 0.28$, $U_{IN} = 2$ m/s, $T_{IN} = 312$ K. Predictions with the catalytic scheme of Deutschmann [20] and the gas-phase schemes of: (b) Warnatz [27], (c) Yetter (Mueller et al. [40]) and (d) Miller and Bowman [41]. The arrows denote the onset of homogeneous ignition. The color bar provides the OH in ppmv and pertains to (a) and (b).

measured temperatures inside the reactor provide only a weighted average between the catalyst surface temperature and the mean gas temperature). The predicted wall temperatures exceed the adiabatic equilibrium temperature ($T_{ad,eq}$) by as much as 200 K while the mean gas temperatures surpass $T_{ad,eq}$ for $x > 27$ mm. This is a result of chemical non-equilibration due to the short convective time scales and the presence of multiple reaction pathways with different time scales (fast oxidation reactions and slow steam reforming). The requirement for accurate catalytic reaction schemes is of the utmost importance for the design of very short contact time reactors: for example, an artificial reduction of the wall temperature by 40 K decreases the computed H_2 yields by 40%. Furthermore, the thermodynamic consistency [39] of the reaction mechanisms deserves special attention. For very short contact time reactors this requirement may not be binding; however, thermodynamic consistency of the catalytic mechanism is essential for longer residence times when products approach equilibration.

3.3. Combustion of hydrogen/air mixtures over Pt

The Raman/OH-LIF methodology has been also applied to investigate the gas-phase chemistry during combustion of fuel-lean ($\varphi \leq 0.32$) H_2/air mixtures over Pt at $p = 1$ bar [3]. Catalytic kinetics were not assessed since the high reactivity of H_2 on Pt led to mass-transport-limited operation. Measured and computed distributions of the OH radical are provided in Fig. 8. The scheme of Warnatz et al. [27] underpredicts the measured homogenous ignition distance (x_{ig}) mildly, while the schemes of Yetter (Mueller et al. [40]) and Miller [41] yield significantly shorter ignition distances. Even for this simple fuel, the corresponding differences in ignition delay times are up to 20 ms, i.e. comparable to the residence times of gas-turbine reactors. The origin of the large x_{ig} differences is largely attributed to the presence of catalytically-formed H_2O [3]. It is finally noted that the catalytically-formed H_2O inhibits chemically the onset of homogeneous ignition [3,42], an effect opposite to that observed in CH_4/air combustion (see Section 3.1.2).

4. Turbulent catalytic combustion

The catalytic reactors of modern large turbines can reach at full-load inlet Reynolds numbers (pertaining to each individual honeycomb channel) of up to 40,000. To attain a CST-relevant ~50% catalytic fuel conversion [43] at those Reynolds numbers, mass transport considerations dictate a channel length that is typically less than one-hundred hydraulic diameters. This leads to spatially developing flows over the entire reactor length. Turbulent CST models should describe accurately the transitional entry channel-flow in the presence of hetero-/homogeneous combustion. Despite their practical importance, such models have not received proper attention and current simulations are mainly based on 1D approaches with lumped transport coefficients. Direct numerical simulation (DNS) or large eddy simulation (LES) have not yet fully advanced in entry channel flows, even for simpler non-reacting cases. This is because the former stresses primarily the temporally and not the spatially developing flows [44] while the latter is hindered by the lack of proper subgrid models for wall-bounded flows [45].

In entry channel flows with heat transfer, the controlling parameters are the magnitude of the incoming turbulence and the laminarization of the flow [46]. In the presence of heat transfer, the near-wall turbulence damping is much stronger compared to that of isothermal flows: the laminarization in the former flows is caused not only by the velocity drop due to wall proximity but also by the viscosity increase due to heat transfer. DNS in the entry region of a heated pipe air-flow at a moderate Re_{IN} of 4300 [47] supplemented with heat transfer experiments

has led to the development of advanced low Reynolds (LR) number models with damping functions suitable for strongly heated and developing channel flows [46]. Comprehensive turbulent CST models were developed only very recently [10–12].

4.1. Turbulent catalytic combustion modeling

A moment closure approach is adopted [10,12], whereby the Favre-averaged transport equation of any gas-phase variable φ becomes:

$$\frac{\partial(\bar{\rho}\tilde{u}\tilde{\varphi})}{\partial x}+\frac{\partial(\bar{\rho}\tilde{v}\tilde{\varphi})}{\partial y}-\frac{\partial}{\partial x}\left(\Gamma_{\text{eff}}\frac{\partial\tilde{\varphi}}{\partial x}\right)-\frac{\partial}{\partial y}\left(\Gamma_{\text{eff}}\frac{\partial\tilde{\varphi}}{\partial y}\right)=\tilde{S}_{\varphi}, \quad (1)$$

$$\Gamma_{\text{eff}}=\Gamma_{\text{l}}+\frac{\mu_{\text{t}}}{\sigma_{\varphi}} \quad \text{and} \quad \mu_{\text{t}}=c_{\mu}f_{\mu}\frac{\bar{\rho}\tilde{k}^2}{\tilde{\varepsilon}}. \quad (2)$$

The governing equations for all first and second order moments are obtained from Eq. (1) [12]. Thermochemical closure for the mean gaseous reaction rates is achieved with a presumed Gaussian-shape joint probability density function (pdf) sub-model. For the catalytic reaction rates, the large thermal inertia of the solid wall suppresses the surface temperature fluctuations and eliminates the major reaction non-linearity. Therefore, the mean catalytic rates are evaluated at the wall temperature [12]. Three different LR turbulence models are tested. The first is the two-layer model of Chen and Patel [48] developed for non-heated flows; it is typical to most isothermal models and allows for direct comparisons with the following heat-transfer LR models. The LR model of Ezato et al. [46] has been validated in strongly laminarizing heated channel flows and the LR model of Hwang and Lin [49] was developed for channel flows with and without heat transfer.

Raman and OH LIF measurements are carried out in H_2/air turbulent combustion over Pt at $p = 1$ bar. In addition, particle image velocimetry (PIV) provides the 2D velocity field along the x–y symmetry plane. The PIV laser sheet has the same orientation as the OH LIF sheet of Fig. 1. PIV data are also acquired in non-reacting isothermal air-flows with inlet Reynolds numbers (Re_{IN}) comparable to those of the reacting cases. The gas-phase scheme or Warnatz [27] (validated in Section 3.3) and the catalytic of Deutschmann [20] are used in the simulations.

4.2. Laminarization in catalytic combustion

Measured and predicted profiles of the mean velocity $\tilde{U}$ and the turbulent kinetic energy $\tilde{k}$ are provided in Fig. 9 for two cases with comparable Re_{IN}: the reacting Case 3 and the non-reacting Case 4. In the latter case, the two-layer model [48] provides very good agreement with the measurements. On the other hand, the heat-transfer models of Hwang and Lin [49] and particularly Ezato et al. [46] underpredict (overpredict) to a large extent $\tilde{k}$ ($\tilde{U}$) as seen in Fig. 9((a) and (b)). Those models are overdissipative, clearly demonstrating the applicability of the two-layer model and the inapplicability of the heat transfer LR models in isothermal channel-flows.

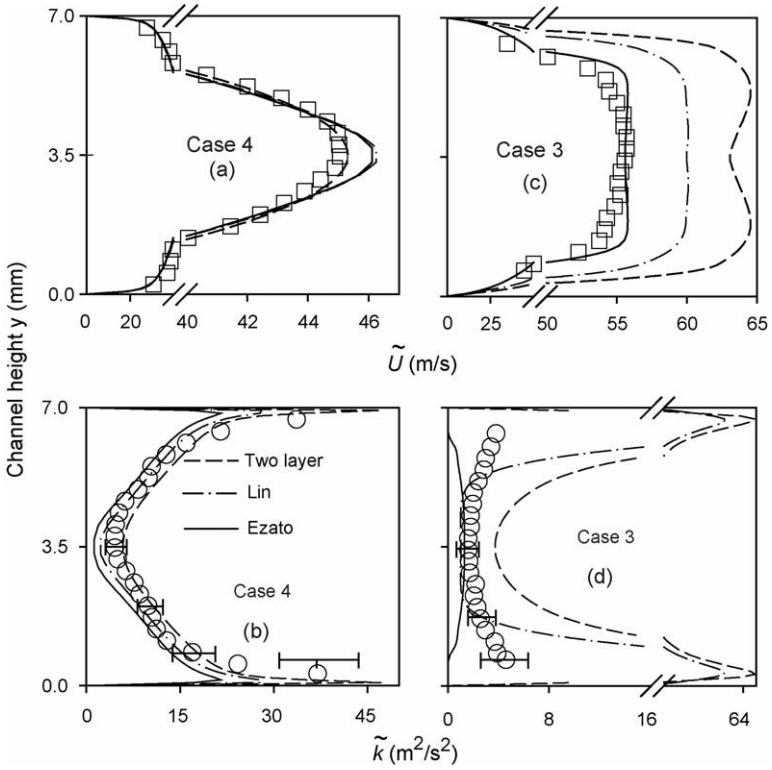

Fig. 9. Transverse profiles at $x = 195$ mm, of: Favre-average axial velocities $\tilde{U}$ (a and c), and turbulent kinetic energies $\tilde{k}$ (b and d) for the reacting Case 3 (see legend of Fig. 11) and the non-reacting Case 4 (300 K air-flow with $Re_{\text{IN}} = 35{,}240$), adapted from [12]. The symbols are PIV measurements and the lines are predictions with different LR turbulence models.

The surface temperatures in the reacting Case 3 exceed 1200 K. Ezato's model provides good agreement to the measured $\tilde{U}$ (Fig. 9c), while the model of Hwang and Lin [49], and to a greater extent the two-layer [48], overpredicts $\tilde{U}$ substantially. Detailed comparisons [12] indicate that $\tilde{k}$ decreases with increasing x and only Ezato's model captures this trend, although it underpredicts somewhat the measured near-wall $\tilde{k}$ (see Fig. 9d). The Hwang and Lin [49], and particularly the two-layer model [48], yield considerably higher near-wall $\tilde{k}$ levels that enhance the transport of heat from the hot wall to the channel core, thereby accelerating unrealistically the mean flow (Fig. 9c). Therefore, isothermal models cannot describe turbulent CST and from the tested heat-transfer models only that of Ezato provides a realistically strong turbulence damping.

4.3. Interaction of turbulence and hetero-/homogeneous combustion

Predicted local catalytic (C) and gas-phase (G) Favre-average hydrogen conversion rates are presented in Fig. 10 for Case 3 of Fig. 9; the shaded area defines the post-homogeneous-ignition zone ($x > x_{ig}$) as predicted by the model of Ezato. Laminar simulations are also included, whereby the boundary conditions (mean inlet velocities and surface temperatures) are kept the same but turbulence is turned-off. The circles with the error bars provide the Raman-measured total (catalytic and gaseous) H_2 average conversion rates. The measured homogeneous ignition (deduced from the OH-LIF distributions of Fig. 11) is marked by $x_{ig,m}$ and that predicted from laminar modeling by $x_{ig,l}$.

Fig. 10 illustrates that H_2 is converted solely by the catalytic pathway at $0 \leq x \leq x_{ig}$. The model of Ezato et al. [46] provides good agreement to the measured C conversion while the Hwang and Lin [49] and two-layer [48] models yield significant overpredictions. This is due to their overestimate in $\tilde{k}$ (Fig. 9d)

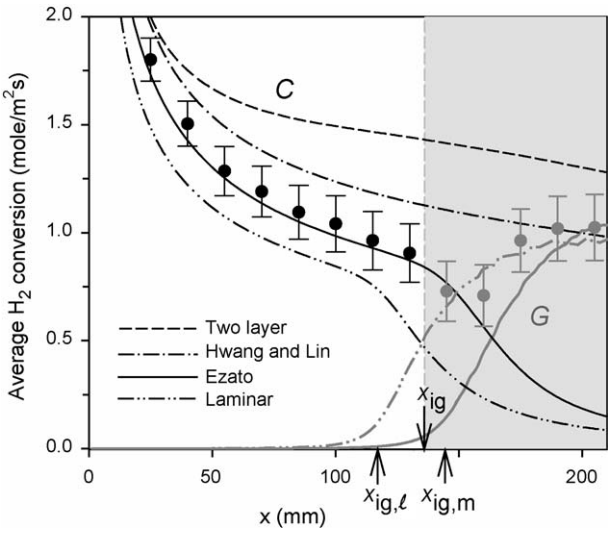

Fig. 10. Raman-measured (circles with error bars) and predicted (lines) Favre-average H_2 conversion rates for Case 3 (see legend of Fig. 11), adapted from [12]. The predicted catalytic (C) and gaseous (G) conversions are shown in black and gray lines, respectively.

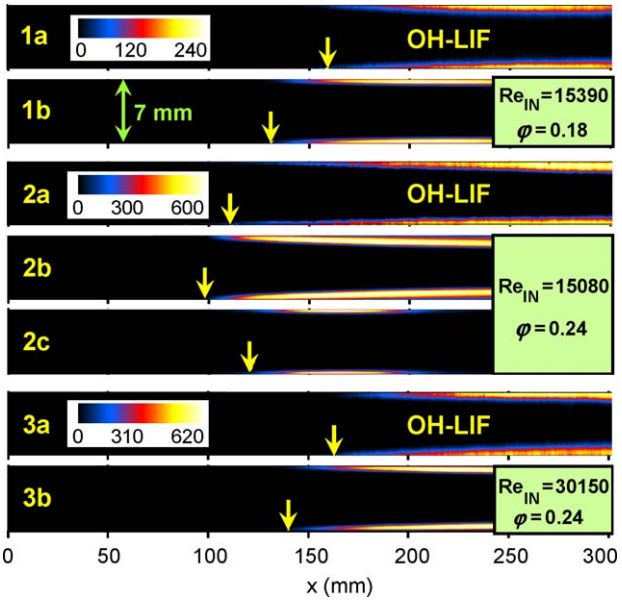

Fig. 11. LIF-measured (a) and predicted (b and c) OH maps, adapted from [11,12]. Case 1: $\varphi = 0.18$, $\tilde{U}_{IN} = 20$ m/s, $Re_{IN} = 15{,}390$. Case 2: $\varphi = 0.24$, $\tilde{U}_{IN} = 20$ m/s, $Re_{IN} = 15{,}080$. Case 3: $\varphi = 0.24$, $\tilde{U}_{IN} = 40$ m/s, $Re_{IN} = 30{,}150$. Predictions with the models of: (b) Ezato [46], and (c) Hwang and Lin [49] only for Case 2. The color bars provide the OH in ppmv.

that leads successively to higher effective transport coefficients Γ_{eff} (see Eq. (2)), to increased transverse scalar transport towards the wall and, finally, to enhanced H_2 catalytic consumption. It is clarified that the catalytic chemistry is still fast enough to cope with the enhanced transport of the heat transfer models: simulations have attested mass-transport-limited catalytic conversion for all three models. The model of Ezato [46] underestimates slightly the catalytic hydrogen conversion (Fig. 10), which is indicative of a somewhat stronger laminarization. The laminar computations of Fig. 10 are in closer agreement to the measurements than the predictions of the two-layer model or the inadequately-laminarizing model of Hwang and Lin. This suggests that, under moderate Reynolds numbers, a laminar model may suffice for CST.

Measured and predicted 2D maps of the OH radical are provided in Fig. 11; the predictions refer only to those LR models that captured homogeneous ignition. The model of Ezato [46] reproduces the measured location of homogeneous ignition and the flame shape in all cases. The two-layer model [48] fails to provide homogeneous ignition in all cases. Finally, the model of Hwang and Lin [49] captures ignition only for Case 2, however, with a resulting very short flame length as seen in Fig. 11(2c). The above differences are directly linked to the laminarization of the turbulent flow. The latter two models yield enhanced turbulent transport, leading to increased upstream catalytic conversion (Fig. 10) that deprives H_2 from the homogeneous pathway and also removes efficiently heat from the near-wall hot ignitable mixture. Both factors inhibit homogeneous ignition. Furthermore, the increased turbulent transport has a profound impact on the wall-bounded flames of Fig. 11 by reducing the available residence times across the

gaseous combustion zone. Laminar stagnation-flow catalytic combustion studies [50] have shown that a rise in strain rate pushes the flame against the catalytic wall, leading to incomplete combustion through the gaseous reaction zone and to a subsequent catalytic conversion of the leaked fuel; a further increase in the strain rate extinguishes the flame. Turbulent transport in channel-flows has a role analogous to that of the strain rate in stagnation-flows.

4.4. Implications to practical systems

Using the validated LR model of Ezato, additional computations of H_2/air catalytic combustion over Pt have been carried out in commercial channel geometries at conditions leading up to 80% catalytic fuel conversion [12]. Uniform inlet turbulent kinetic energies and turbulent dissipation rates were used in the simulations, according to:

$$\tilde{k}_{\mathrm{IN}} = \alpha_1 \bar{U}_{\mathrm{IN}}^2 \quad \text{and} \quad \tilde{\varepsilon}_{\mathrm{IN}} = \frac{(c_\mu/\alpha_2) k_{\mathrm{IN}}^{3/2}}{r_{\mathrm{h}}}, \tag{3}$$

with r_{h} the channel hydraulic radius and $\alpha_2 = 0.03$. The computed flow laminarization domains are shown in Fig. 12. In the shaded zones the flow laminarizes and the turbulent H_2 conversion differs by less than 10% from the corresponding conversion of a simpler laminar model. For example, in high-temperature catalysts with $T_{\mathrm{W}} = 1200$ K, turbulence modeling is needed only for $Re_{\mathrm{IN}} > 2.7 \times 10^4$ when $\alpha_1 = 0.005$ and for $Re_{\mathrm{IN}} > 2 \times 10^4$ when $\alpha_1 = 0.05$. The notion of laminarization does not necessarily imply a continuous suppression of turbulence; it rather suggests that the length-to-diameter ratio required for transition to fully turbulent flow exceeds that of practical catalytic reactors. As seen in Fig. 12, the inlet turbulence (determined by the parameter α_1) is crucial in determining the extent of flow laminarization. The memory of inlet turbulence is maintained because of the moderate channel length-to-diameter ratios. It is also evident that turbulent transport models based on lumped Sherwood and Nusselt

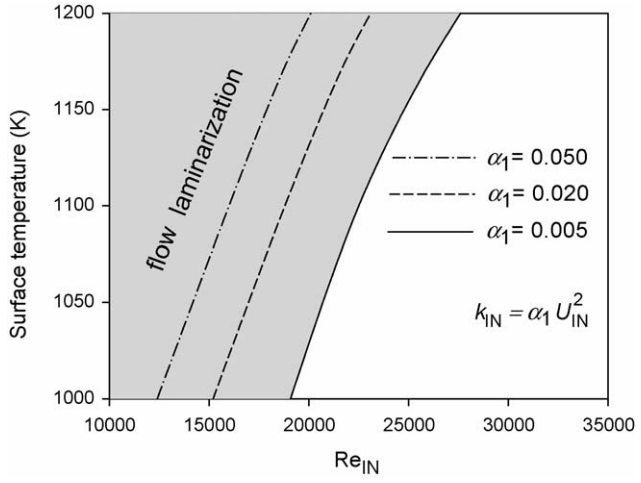

Fig. 12. Domains of flow laminarization in catalytic combustion, adapted from [12]. The lines correspond to different inlet turbulent kinetic energies according to Eq. (3).

transport coefficients cannot account for inlet turbulence effects.

The magnitude of the inlet turbulence in gas-turbine catalytic reactors with individual channel diameters smaller or equal than 1 mm deserves some attention. The inlet turbulence is controlled by the compressor discharge and the fuel/air mixing unit; however, only part of the turbulence spectrum with length scales smaller than the channel diameter can enter the reactor (it is unlikely that the integral length scales of turbulence are less than 1 mm). Spectral energy considerations have shown [51] that precisely those small eddies have a profound impact on combustion. Moreover, anisotropies are expected to arise since the cut-off of the inlet turbulence spectrum will be preferential along the cross-flow directions. DNS is a promising tool for addressing those issues (see Section 5).

A reactant preheat will narrow down the laminarization domains of Fig. 12, which pertain to $T_{\mathrm{IN}} = 300$ K. The presented CST model is valid for steady-state, high-temperature reactor performance ($1000\ \mathrm{K} \leq T_{\mathrm{W}} \leq 1250$ K). Transient behavior, such as catalytic ignition, necessitates the development/validation of LR models that perform adequately over a much wider surface temperature range. The results of Fig. 9 have shown that a single LR turbulent model cannot perform satisfactorily from 300 to 1200 K. Future research should focus on the development of such models, which could aid the design of CST reactors. Another issue of interest in reactors with small channel diameters is the effect of surface roughness. For inlet Reynolds numbers less than 40,000 there is always an extended viscous sublayer near the wall, particularly under high-wall-temperature operation. Therefore, it is anticipated that the surface protrusions will not exceed the viscous sublayer thickness and, therefore, the developed turbulent CST model will hold without any modification. On the other hand, excessive deviations from a smooth channel wall (not in terms of surface roughness but rather in terms of manufacturing imperfections) will affect not only turbulence but also the bulk flow due to the associated small channel diameters. Finally, the plane channel-flow model of Section 4.1 is also valid for most practical systems: honeycomb reactors have 3D channel geometries but the associated secondary flows are in most cases rather weak.

5. Future directions in thermofluidic modeling

Transient models are required for the description of catalytic ignition and of kinetically-driven dynamic oscillatory phenomena. The development of such models poses severe challenges since many physicochemical processes with disparate spatio-/temporal scales must be considered. The relevant time scales range from fractions of ms (gaseous and surface chemical times) to seconds (solid substrate heat-up time). Fully transient models with detailed chemistry are currently only 1D. A 2D model, on the other hand, provides accurate description of the interphase transport, hence eliminating potential falsification of the surface kinetics. Moreover, it can resolve the gas-phase species boundary layers that may be of importance in certain

catalytic processes. Current transient 2D models invoke the quasisteady assumption for the gas-phase. This assumption does not necessarily hold during light-off, wherein the chemical times become comparable to the solid (heat conduction) time scale. A fully transient laminar 2D code (denoted as laminar DNS) will greatly aid the understanding of the interplay between chemistry and transport during light-off. DNS has progressed during the last years in gaseous combustion and an extension to hetero-/homogeneous combustion is under way [52]. Moreover, DNS can elucidate the turbulent heat and mass transport and assess the impact of inlet turbulence and flow laminarization on the in-channel processes such that salient engineering models can be developed. Turbulent DNS of catalytic channel-flows is feasible for inlet Reynolds numbers up to ∼5000.

An issue of interest in technical catalysts is the modeling of intraphase diffusion. Current models define an effective diffusivity by combining Knudsen and molecular diffusion, and describe the porous transport with macroscopic approaches such as the dusty gas model. New numerical tools suited for micro-/mesoscale flows (Knudsen numbers up to 0.1) include the lattice Boltzmann (LB) models. LB involves solution of discrete velocity distributions and is well-suited for micro-channels. Methodologies for extending the LB formulation to multi-species flows have been recently advanced [53]. LB models can elucidate the physicochemical processes in microchannels and porous media with surface reactions, can be further incorporated as submodels in larger CFD codes, and can refine existing macroscopic models.

6. Conclusions

The hetero-/homogeneous chemistry and its coupling to transport have been reviewed. The advent of in situ, locally-resolved measurements of major and minor gas-phase species concentrations over the catalyst boundary layer has opened new directions for the study of catalytic combustion. Those techniques furnished a salient methodology for the study of chemistry and its coupling to transport that will probably extend well-beyond the time that surface science develops true in situ measuring techniques for combustion environments.

Recent studies have provided validated hetero-/homogeneous reaction schemes for fuel-lean combustion of hydrogen and methane over platinum and assessed the coupling of the two pathways. Even for those relatively simple fuels, the underlying kinetics were previously not well understood. It was shown that the hetero-/homogeneous radical coupling inhibits only mildly the onset of homogeneous ignition. The catalytic reactivity of fuel-lean methane/air mixtures over platinum increases with rising pressure but the rate of increase is moderated by the corresponding decrease in surface free sites. Similar kinetic investigations are also reported for fuel-rich partial catalytic oxidation of methane over rhodium. Future extension of this methodology to higher hydrocarbons is highly desirable for applications that include micro-combustors and fuel reforming.

For the small aspect ratios of catalytic channels, the turbulent transport is controlled by the flow laminarization induced by the hot catalytic walls. Near-wall turbulence models adapted from the recent heat transfer literature describe adequately the degree of relaminarization only under intense wall heat transfer. Under high-temperature catalytic combustion applications, the domains of laminarization have been mapped out in terms of the inlet turbulent flow properties and the channel wall temperature. Further model development is needed for turbulent catalytic combustion applications with disparate ranges of heat transfer and wall temperatures. Finally, new modeling directions that include direct numerical simulation for transient simulations and lattice Boltzmann techniques for transport in porous media appear promising for catalytic combustion.

Acknowledgements

Support was provided by the Swiss Federal Office of Energy (BFE), Swiss Federal Office of Education and Technology (BBT), European Union and ALSTOM Power.

References

[1] T.A. Griffin, M. Calabrese, L.D. Pfefferle, A. Sappey, R. Copeland, D.R. Crosley, Combust. Flame 90 (1992) 11.
[2] M. Reinke, J. Mantzaras, R. Schaeren, R. Bombach, A. Inauen, S. Schenker, Combust. Flame 136 (2004) 217.
[3] C. Appel, J. Mantzaras, R. Schaeren, R. Bombach, A. Inauen, B. Kaeppeli, B. Hemmerling, A. Stampanoni, Combust. Flame 128 (2002) 340.
[4] M. Reinke, J. Mantzaras, R. Schaeren, R. Bombach, A. Inauen, S. Schenker, Proc. Combust. Inst. 30 (2005) 2519.
[5] U. Dogwiler, J. Mantzaras, P. Benz, B. Kaeppeli, R. Bombach, A. Arnold, Proc. Combust. Inst. 27 (1998) 2275.
[6] M. Reinke, J. Mantzaras, R. Schaeren, R. Bombach, W. Kreutner, A. Inauen, Proc. Combust. Inst. 29 (2002) 1021.
[7] M. Reinke, J. Mantzaras, R. Bombach, S. Schenker, A. Inauen, Combust. Flame 141 (2005) 448.
[8] C. Appel, J. Mantzaras, R. Schaeren, R. Bombach, A. Inauen, N. Tylli, M. Wolf, T. Griffin, D. Winkler, R. Carroni, Proc. Combust. Inst. 30 (2005) 2509.
[9] A. Schneider, J. Mantzaras, P. Jansohn, Chem. Eng. Sci. 61 (2006) 4634.
[10] J. Mantzaras, C. Appel, P. Benz, U. Dogwiler, Catal. Today 59 (2000) 3.
[11] C. Appel, J. Mantzaras, R. Schaeren, R. Bombach, B. Kaeppeli, A. Inauen, Proc. Combust. Inst. 29 (2002) 1031.
[12] C. Appel, J. Mantzaras, R. Schaeren, R. Bombach, A. Inauen, Combust. Flame 140 (2005) 70.
[13] G.A. Somorjai, G. Rupprechter, J. Phys. Chem. B 103 (1999) 1623.
[14] R. Kissel-Osterrieder, F. Behrendt, J. Warnatz, U. Metka, H.R. Volpp, J. Wolfrum, Proc. Combust. Inst. 28 (2000) 1341.
[15] J.G. McCarty, Catal. Today 26 (1995) 283.
[16] G. Groppi, W. Ibashi, E. Tronconi, P. Forzatti, Catal. Today 69 (2001) 399.
[17] M. Lyubovsky, L. Pfefferle, Catal. Today 47 (1999) 29.
[18] X. Song, W.R. Williams, L.D. Schmidt, R. Aris, Combust. Flame 84 (1991) 292.
[19] H. Ikeda, J. Sato, F.A. Williams, Surf. Sci. 326 (1995) 11.
[20] O. Deutschmann, R. Schmidt, F. Behrendt, J. Warnatz, Proc. Combust. Inst. 26 (1747).
[21] P. Aghalayam, Y.K. Park, D.G. Vlachos, Proc. Combust. Inst. 28 (2000) 1331.
[22] R.W. Sidwell, H.Y. Zhu, R.J. Kee, D.T. Wickham, Combust. Flame 134 (2003) 55.
[23] M.E. Coltrin, R.J. Kee, G.H. Evans, E. Meeks, F.M. Rupley, J.M. Grcar, Report No. SAND 91-8003, Sandia National Laboratories, Livermore, CA, 1996.
[24] J.D. Taylor, M.D. Allendorf, A.H. McDaniel, S.F. Rice, Ind. Eng. Chem. Res. 42 (2003) 6559.

[25] U. Dogwiler, P. Benz, J. Mantzaras, Combust. Flame 116 (1999) 243.
[26] O. Deutschmann, L.I. Maier, U. Riedel, A.H. Stroemman, R.W. Dibble, Catal. Today 59 (2000) 141.
[27] J. Warnatz, R.W. Dibble, U. Maas, Combustion Physical and Chemical Fundamentals Modeling and Simulation, Springer-Verlag, New York, 1996.
[28] C.K. Westbrook, F.L. Dryer, Combust. Sci. Technol. 27 (1981) 31.
[29] H.K. Moffat, P. Glaborg, R.J. Kee, J.F. Grcar, J.A. Miller, Report No. SAND91-8001, Sandia National Laboratories, Livermore, USA, 1993.
[30] J. Mantzaras, C. Appel, Combust. Flame 130 (2002) 336.
[31] G.P. Smith, D.M. Golden, M. Frenklach, N.W. Moriarty, B. Eiteneer, M. Goldenberg, C.T. Bowman, R.K. Hanson, S. Song, W.C. Gardiner, V. Lissianski, Z. Qin, An Optimized Detailed Chemical Reaction Mechanism for Methane Combustion, Gas Research Institute, 2000 http://www.me.berkeley.edu/gri_mech.
[32] K.J. Hughes, T. Turanyi, A. Clague, M.J. Pilling, Int. J. Chem. Kinet. 33 (2001) 513.
[33] G. Friedrichs, J.T. Herbon, D.F. Davidson, R.K. Hanson, Phys. Chem. Chem. Phys. 4 (2002) 5778.
[34] R. Carroni, T. Griffin, J. Mantzaras, M. Reinke, Catal. Today 83 (2003) 157.
[35] T. Griffin, D. Winkler, M. Wolf, C. Appel, J. Mantzaras, ASME (2004) 54101.
[36] M.J. Castaldi, S. Etemed, W.C. Pfefferle, V. Khanna, K.O. Smith, J. Eng. Gas. Turbines Power-Trans. ASME 127 (2005) 27.
[37] R. Schwiedernoch, S. Tischer, C. Correa, O. Deutschmann, Chem. Eng. Sci. 58 (2003) 633.
[38] A. Schneider, J. Mantzaras, R. Bombach, S. Schenker, N. Tylli, P. Jansohn, Laser induced fluorescence of formaldehyde and Raman measurements of major species during partial catalytic oxidation of methane with large H_2O and CO_2 dilution at pressures up to 10 bar, Thirty–first International Symposium on Combustion, Heidelberg, Germany, August 6–11, (2006).
[39] A.B. Mhadeshwar, H. Wang, D.G. Vlachos, Abstr. Pap. Am. Chem. Soc. 226 (2003) 11.
[40] M.A. Mueller, T.J. Kim, R.A. Yetter, F.L. Dryer, Int. J. Chem. Kinet. 31 (1999) 113.
[41] J.A. Miller, C.T. Bowman, Prog. Energy Combust. Sci. 15 (1989) 273.
[42] P.A. Bui, D.G. Vlachos, P.R. Westmoreland, Proc. Combust. Inst. 26 (1763).
[43] R.A. Dalla Betta, T. Rostrup-Nielsen, Catal. Today 47 (1999) 369.
[44] T. Poinsot, S. Candel, A. Trouve, Prog. Energy Combust. Sci. 21 (1996) 531.
[45] C. Haertel, L. Kleiser, J. Fluid Mech. 356 (1998) 327.
[46] K. Ezato, A.M. Shehata, T. Kunugi, D.M. McEligot, J. Heat Transf. – Trans. ASME 121 (1999) 546.
[47] S. Satake, T. Kunugi, A.M. Shehata, D.M. McEligot, Int. J. Heat Fluid Flow 21 (2000) 526.
[48] H.C. Chen, V.C. Patel, AIAA J. 26 (1988) 641.
[49] C.B. Hwang, C.A. Lin, AIAA J. 36 (1998) 38.
[50] C.K. Law, G.I. Sivashinsky, Combust. Sci. Technol. 29 (1982) 277.
[51] J. Mantzaras, Combust. Sci. Technol. 86 (1992) 135.
[52] J. Mantzaras, C.E. Frouzakis, K. Boulouchos, in preparation.
[53] S. Arcidiacono, S. Ansumali, I.V. Karlin, J. Mantzaras, K. Boulouchos, Entropic lattice Boltzmann method for simulation of binary mixtures, Mathematics and Computerts in Simulation, 2006. in press.